Appl. Phys. B 74 [Suppl.], S237–S243 (2002)
DOI: 10.1007/s00340-002-0886-8

Applied Physics B
Lasers and Optics

L. GALLMANN[1,✉]
G. STEINMEYER[1]
G. IMESHEV[2,*]
J.-P. MEYN[3]
M.M. FEJER[2]
U. KELLER[1]

Sub-6-fs blue pulses generated by quasi-phase-matching second-harmonic generation pulse compression

[1] Ultrafast Laser Physics Laboratory, Institute of Quantum Electronics, Swiss Federal Institute of Technology, ETH Hönggerberg – HPT, 8093 Zürich, Switzerland
[2] E.L. Ginzton Laboratory, Stanford University, Stanford, CA 94305, USA
[3] Fachbereich Physik, Universität Kaiserslautern, 67663 Kaiserslautern, Germany

Received: 17 September 2001/
Revised version: 27 November 2001
Published online: 27 June 2002 •

ABSTRACT We demonstrate a novel scalable and engineerable approach for the frequency-doubling of ultrashort pulses. Our technique is based on quasi-phase-matching and simultaneously provides tailored dispersion and nonlinear frequency conversion of few-cycle optical pulses. The method makes use of the spatial localization of the conversion process and the group velocity mismatch in a chirped grating structure. The total group delay of the nonlinear device can be designed to generate nearly arbitrarily chirped second-harmonic pulses from positively or negatively chirped input pulses. In particular, compressed second-harmonic pulses can be obtained. A brief summary of the underlying theory is presented, followed by a detailed discussion of our experimental results. We experimentally demonstrate quasi-phase-matching pulse compression in the sub-10-fs regime by generating few-cycle pulses in the blue to near-ultraviolet spectral range. Using this new frequency conversion technique, we generate sub-6-fs pulses centered at 405 nm by second-harmonic generation from a 8.6 fs Ti:sapphire laser pulse. The generated spectrum spans a bandwidth of 220 THz. To our knowledge, these are the shortest pulses ever obtained by second-harmonic generation.

PACS 42.65.Ky; 42.65.Re; 42.79.Nv

1 Introduction

Nowadays, sub-10-fs optical pulses are routinely generated using Ti:sapphire laser oscillators, with the shortest pulses demonstrated so far having a sub-6-fs duration [1–3]. But many applications, especially in spectroscopy, require sub-10-fs pulses outside the Ti:sapphire gain bandwidth. With such short pulses, these spectral regions can only be accessed by means of frequency conversion processes, which are, to date, always driven by Ti:sapphire-based laser systems. Three fundamentally different methods have been demonstrated that produce sub-10-fs pulses in the blue to near-ultraviolet spectral region: self-phase-modulation in an argon-filled hollow-core fiber [4], phase-locked Raman sideband generation [5], and second-harmonic generation (SHG) [6, 7]. The first two techniques use spectral broadening and subsequent compression of the second harmonic (SH) of amplified pulses from a Ti:sapphire laser system and are therefore restricted to kHz repetition rates. If large pulse energies are not required, SHG offers the advantage of MHz repetition rates and thus the potential for very sensitive measurements in spectroscopy.

The classical approach to frequency-doubling of ultrashort pulses is the use of birefringent phase-matching in short nonlinear optical crystals. Birefringent phase-matching can be achieved only for a very limited number of nonlinear optical materials and a limited range of phase-matchable wavelengths. Restriction of the interaction length is required in order to minimize the group velocity mismatch (GVM) between the fundamental pulse and its second harmonic. The temporal walk-off between these two pulses has to be kept below the pulse duration. Decreasing the GVM in the nonlinear interaction increases the conversion bandwidth [8]. For frequency-doubling of sub-10-fs pulses from a Ti:sapphire laser, this limits the length of the nonlinear crystal to typically less than $\sim 50\,\mu$m, depending on the exact dispersion properties of the material. Apart from practical problems of polishing and handling such thin crystals, it is usually difficult to focus sub-10-fs pulses confocally into these crystals. Looser focusing generally results in poor conversion efficiencies. Using birefringent phase-matching, blue pulses with durations of 10 fs [9] and 8 fs [6] were generated recently by doubling of ~ 10 fs pulses from a Ti:sapphire oscillator. In [6], focusing the first harmonic (FH) tighter than confocally into a 100-μm-thick BBO crystal reduced the effective nonlinear interaction length and alleviated SH pulse broadening owing to GVM. 80 mW of SH light was generated, with 950 mW FH power and an efficiency of 0.7%/nJ. Very recently, a novel technique has been proposed that should allow compression of the fundamental pulse into a few-fs second-harmonic pulse using birefringent type-II phase-matching in a thick nonlinear crystal [10]. This method requires strong depletion of the first harmonic (FH). However, for this method there exists no experimental data in the sub-10-fs regime so far.

In this paper we describe an alternative approach to frequency-doubling of sub-10-fs pulses that does not suffer from the crystal length and focusing limitations. Our method relies upon quasi-phase-matching (QPM, [11, 12]), which

✉ Fax: +41-1/633-1059, E-mail: gallmann@iqe.phys.ethz.ch
*_Present address_: Scion Photonics, 345 Los Coches St., Milpitas, CA 95035, USA

can be engineered to provide dispersion compensation of ultrashort pulses [13, 14]. Microstructured QPM crystals have been used extensively in frequency conversion devices. The proven advantages of such devices over conventional birefringent materials are non-critical phase-matching, the use of large nonlinearities, and high conversion efficiencies. Tailoring of the amplitude and phase response of the device (see e.g. [15, 16]) is a novel aspect, which makes QPM crystals a particularly attractive nonlinear medium for the frequency conversion of sub-10-fs pulses. Using QPM-SHG pulse compression, we were able to generate sub-6-fs SH pulses and thus demonstrated the scalability of this QPM-based technique to shorter pulse durations [7]. In the following, we give a schematic description of our method together with an analytical theory for the design of the QPM gratings, followed by a detailed discussion of the experimental results and techniques.

2 QPM-SHG pulse compression

2.1 *Simple time-domain picture*

QPM-SHG pulse compression can be most intuitively explained in the time domain under assumption of spatial localization of the frequency conversion process [13, 17]. This assumption means that any given wavelength of the input pulse is frequency-doubled at one particular position inside the crystal. It has been shown that this treatment holds under a more rigorous analysis of the nonlinear propagation and conversion and that it allows to correctly compute the spectral phase of the output pulse [14]. Let us now start with the additional simplifying assumption that material dispersion beyond GVM is negligible. We will later relieve this assumption and extend the discussion to arbitrary dispersion order.

Figure 1 schematically illustrates the basic principle of QPM-SHG pulse compression in the time domain. In this example, it is assumed that a positively prechirped fundamental pulse is to be converted into a transform-limited SH pulse. The FH pulse enters the QPM crystal from the left and propagates at the fundamental group velocity. First the long wavelengths in the front section of the pulse become frequency-doubled as soon as they reach the position where the local QPM grating period phase-matches this process. The frequency-doubled components propagate at the SH group velocity, which in this case is assumed to be smaller than the fundamental one. Because of this difference in propagation speed, the short wavelengths in the trailing edge of the input pulse catch up with the previously frequency-doubled portions. If the chirp of the QPM grating matches the chirp of the input pulse, the SH of these short-wavelength components can be made to exactly temporally overlap the previously generated SH pulse. As a result, one observes a compressed SH pulse at the output of the QPM crystal.

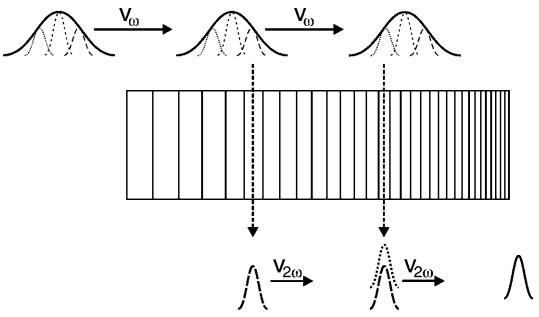

FIGURE 1 Schematic picture of QPM-SHG pulse compression: The positively chirped fundamental pulse enters the grating from the left and travels at the fundamental group velocity. The long-wavelength components (*long dashes*) get converted as soon as they arrive at the proper QPM period. Their SH travels at the slower SH group velocity. Thus, the short-wavelength components (*short dashes*) of the FH pulse can catch up. If the grating chirp is chosen correctly the SH of the short-wavelength component will exactly temporally overlap the previously doubled parts and, therefore, a compressed SH pulse will exit the grating

Converting a positively chirped fundamental into an unchirped SH pulse is only one of many different chirp configurations that can be achieved with this approach. The input pulse can carry either a non-vanishing positive or negative chirp; the output pulse can have an arbitrary chirp. Of interest in ultrafast optics, for example, is the generation of negatively prechirped SH output pulses that can be compressed at the position of an experiment by transmission through an appropriate amount of positive dispersion material. This allows compensation of material dispersion on both sides of the frequency conversion device. The possibility to design such chirp configurations is especially interesting because conventional dispersion compensation schemes generally fail for wide bandwidths and short wavelengths. It is important to note here that the magnitude of the SH chirp does not affect the conversion efficiency, which for confocal focusing depends solely on the FH chirp and material properties [17]. Finally, it is not only possible to design the phase response of a QPM-SHG pulse compression device but one can control the spectral amplitudes of the SH pulse by adjusting the duty-cycle of the QPM domains.

2.2 *Analytical QPM grating design theory*

A rigorous theory of QPM-SHG pulse compression in the regime of negligible higher-order dispersion at the FH was given in [17]. This theory was recently extended to account for arbitrary dispersion [14], which thus enables the application of this technique to much shorter pulses. In the following we give a brief description of the design procedure for the chirped QPM grating structure based on [14]. This design procedure relies on the undepleted pump approximation, the slowly varying amplitude approximation and the localization of the conversion process. Furthermore, the equations are given for a non-critical beam geometry, i.e. for collinear wave vectors and energy flow. This is the geometry that is usually chosen with QPM.

The spatial localization of the frequency conversion yields a direct correspondence $z(\omega)$ between position and frequency. This allows one to define the grating period $\Lambda(z)$ of the chirped QPM grating structure as

$$\Lambda(z) = 2\pi m/\Delta k, \quad \Delta k = 2k\left(\frac{\omega}{2}\right) - k(\omega)\ . \tag{1}$$

Here Δk is the wavenumber mismatch between FH and SH as imposed by the material dispersion of the nonlinear optical material. In the following we restrict ourselves to first-order QPM ($m = 1$).

We define the function $z_0(\omega)$ describing the position of conversion of a particular Fourier component of the SH pulse. The goal is to find a function $z_0(\omega)$ such that the total group delay experienced during propagation and conversion yields the desired spectral phase of the second harmonic (up to an unimportant constant phase).

Calculation of the total group delay has to include the phase of the input pulse, propagation of the nonlinear polarization driven by the fundamental pulse up to the conversion point z_0 and the linear propagation of the SH light itself. The spectral phase of the SH components generated at z_0 can be calculated from the phase of the nonlinear polarization P_{NL}, which can be written as a spectral autoconvolution

$$P_{\mathrm{NL}}(z_0,\omega) = \int_{-\infty}^{\infty} E^{(\mathrm{fund})}(z=0,\omega')E^{(\mathrm{fund})}(z=0,\omega-\omega') \times \exp\left[-\mathrm{i}\left(k\left(\omega'\right)+k\left(\omega-\omega'\right)\right)z_0\right]\mathrm{d}\omega' . \quad (2)$$

Here the dispersion of the nonlinear optical material is included as $k(\omega)=\frac{\omega}{c}n(\omega)$ to arbitrary order. An arbitrary prechirp on the FH pulse is considered in the phase of the complex input field $E^{(\mathrm{fund})}_{\mathrm{input}}(z=0,\omega)$. From the conversion point z_0 on, dispersion acting on the generated SH has to be added, giving rise to the total group delay, i.e. the first derivative of the spectral phase with respect to angular frequency, at the output facet of the device

$$\tau_{\mathrm{G}}(z_0,\omega) = \frac{\partial}{\partial\omega}\mathrm{Arg}\left[P_{\mathrm{NL}}(z_0,\omega)\right] + \frac{\partial k(\omega)}{\partial\omega}(L-z_0) . \quad (3)$$

Selection of a particular dependence $z_0(\omega)$ now allows to calculate the group delay of the generated SH pulse from (3). This relationship can be inverted to determine $z_0(\omega)$ for a desired spectral phase of the SH output by demanding $\tau_{\mathrm{G}}(z_0(\omega),\omega)=\frac{\partial}{\partial\omega}\varphi^{(\mathrm{SH})}(\omega)$. To obtain a transform-limited SH output pulse, for example, the relation $\tau_{\mathrm{G}}(z_0(\omega),\omega)=\mathrm{const.}$ must be fulfilled. The inverse function $\omega(z)$ can finally be used to compute the poling period $\Lambda(z)$ from (1).

This design procedure allows compensating for an arbitrary chirp on the input pulse and for arbitrary material dispersion of the nonlinear material. It requires knowledge of the spectral phase of the input pulse and, more importantly, precise data for the dispersion of the materials employed. In practice, knowledge of the input spectral phase is not crucial because it is a good approximation to assume that the QPM grating adds a given phase independent of the input pulse [14].

3 Experiments

QPM-SHG pulse compression was first theoretically and experimentally demonstrated in the regime of negligible dispersion beyond GVM [13, 15]. Such nonlinear devices soon found application in chirped-pulse-amplification-based fiber amplifiers [18]. These experiments were all performed at pulse durations longer than about 100 fs. In this regime higher-order dispersion could be neglected. Using the generalized theory described in the previous section and derived in [14], we were able to reduce pulse durations in QPM-SHG pulse compression by more than one order of magnitude.

For the first experimental demonstration of this new theory, a first-order QPM grating was designed that converts a ~ 20 times positively chirped FH pulse into a compressed SH pulse. This grating was fabricated in a 300-μm-thick congruent $LiTaO_3$ substrate by electric field poling. $LiTaO_3$ was chosen instead of the more common $LiNbO_3$, because it has a deeper UV absorption edge, which makes two-photon absorption of the SH of less concern. Additionally, small QPM periods can be fabricated in this material. The Sellmeier equation of $LiTaO_3$ is accurately known for the UV through infrared spectral range [19]. The group velocity dispersion (GVD) coefficients of $LiTaO_3$ are 305 $\mathrm{fs}^2/\mathrm{mm}$ at the FH and 1140 $\mathrm{fs}^2/\mathrm{mm}$ at the SH and hence GVD effects are substantial already for modest path lengths inside the nonlinear medium. The temporal walk-off length for the 8.6 fs pulses at 810 nm employed in our measurements amounts to only ~ 6 μm. A chirped grating length of 310 μm was used to achieve pulse compression. The local grating $\boldsymbol{K}$-vector was changing nonlinearly with propagation distance, covering QPM periods from 6.5 μm to 1.8 μm. The nonlinearity of this chirp is a direct consequence of the higher-order dispersion terms accounted for in the design procedure. The grating design is depicted in Fig. 2. For this grating the expected conversion efficiency was $\sim 2\%/\mathrm{nJ}$ assuming confocal focusing and ideal poling quality. Other gratings, designed for a smaller FH prechirp, offer as much as $20\%/\mathrm{nJ}$ theoretical efficiency, but were not explored in these experiments. This was done in order to avoid potential complications with two-photon absorption or self-phase-modulation in this first experimental demonstration of our technique.

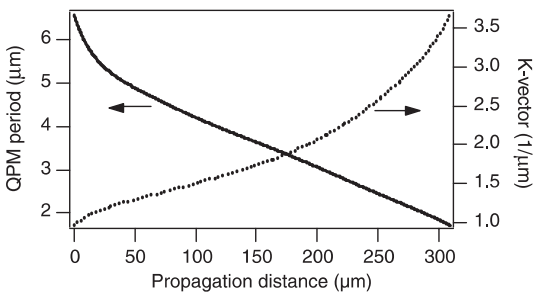

FIGURE 2 QPM period (*solid*) and grating $\boldsymbol{K}$-vector (*dotted*) for the grating design used in our experiments. The deviations from a linear grating chirp are a consequence of the higher-order dispersion in the nonlinear medium

3.1 *Broadband pulse characterization at the second harmonic of* Ti*:sapphire*

The characterization of low-energy sub-10-fs pulses in the blue to near-ultraviolet spectral range is rather challenging. The main reason for this is the increased dispersion of most transparent optical materials at these wavelengths. As a result, most pulse characterization techniques based on autocorrelation-like $\chi^{(2)}$-interactions cannot be operated in this spectral region since broadband phase-matching is not possible anymore in common nonlinear materials. This already rules out the direct use of autocorrelation or SHG frequency-resolved optical gating (SHG-FROG, [20]). For the same reason, spectral phase interferometry for direct electric field reconstruction (SPIDER, [21]) employing upconversion

of the SH pulses with a quasi-cw portion of a strongly chirped SH pulse cannot be applied in this case.

But there are other techniques based on $\chi^{(2)}$-processes for a less direct pulse characterization. These methods use the sum-frequency mixing between the FH and the SH. Such techniques are, for example, the traditional intensity cross-correlation, cross-correlation-FROG (XFROG, [22]) and SPIDER (for sub-10-fs cross-correlation SPIDER, see e.g. [23]) based on the mixing of the SH with a quasi-cw portion of a FH pulse. XFROG and cross-correlation require a well-characterized FH reference pulse. XFROG and SPIDER allow reliable amplitude and phase characterization of the SH pulse, but since they both spectrally disperse the signal they need higher SH power levels than the traditional cross-correlation. Because of its simplicity and high sensitivity, we decided to use intensity cross-correlation to measure our pulses.

3.2 *Extraction of the SH pulse from the cross-correlation measurement*

Traditionally, only a small fraction of the information content of a cross-correlation measurement is used to estimate the pulse duration of one of the pulses if the duration of the other is known. Assuming a certain pulse shape for the two cross-correlated pulses, one obtains the SH pulse duration from the independently measured FH pulse width and the width of the cross-correlation function. This approach is very questionable in the sub-10-fs regime, as pulses can exhibit rather complex shapes. We therefore applied two different iterative decorrelation algorithms on the measured data to extract the full pulse shape of the SH pulse. The two algorithms are schematically depicted in Fig. 3.

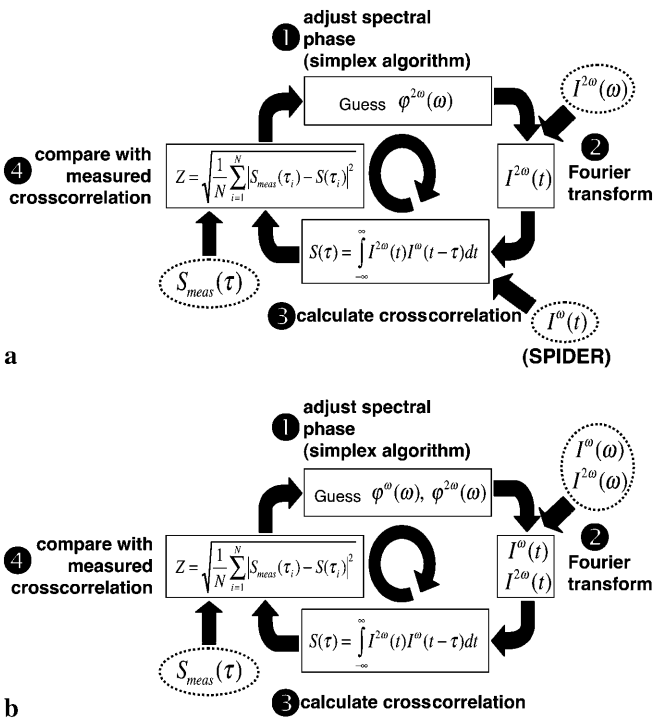

FIGURE 3 Algorithms for the retrieval of the SH pulse from the measured cross-correlation. **a** Algorithm 1 and **b** algorithm 2 mainly differ in the set of input and optimization parameters

Algorithm 1 uses the cross-correlation, the SH spectrum and the temporal pulse shape of the FH reference pulse as the input. The reference pulse is measured with SPIDER [21, 24]. The algorithm is initialized with a random guess for the spectral phase of the SH. With the measured SH spectrum and a Fourier transform, the corresponding temporal pulse shape is obtained. From the guess for the SH pulse shape and the measured FH pulse shape the expected cross-correlation is calculated. This trace is compared to the measured cross-correlation function. The multidimensional downhill simplex method (see [25]) is used to find the spectral phase of the SH pulse that minimizes the mean square deviation between the reconstructed and the measured cross-correlation function. Once the optimization stagnates, the error metric is switched from mean square deviation to the mean absolute deviation. In the presence of experimental noise, this strategy was found to yield a slightly improved agreement in the wings of the cross-correlation compared to the mean square optimization alone, without sacrificing agreement around zero delay.

Algorithm 2 utilizes a reduced input data set consisting of the cross-correlation trace, the FH spectrum and the SH spectrum. In this method the multidimensional optimization is applied to the FH and the SH spectral phase simultaneously. The subsequent part of the algorithm remains the same as for algorithm 1. A similar algorithm was previously demonstrated for autocorrelation measurements in [26]. Algorithm 2 is expected to be much more susceptible to stagnation or to yield incorrect results. In fact, this behavior was observed in several tests using synthetic input data. Best convergence was found in the presence of moderate noise on the input data and with a difference in pulse duration between FH and SH of less than a factor two. For our experimental data, the two algorithms delivered nearly identical results, which generally did not depend on the starting parameters. We thus conclude that both algorithms converged properly. An accidental agreement is very unlikely to occur since the algorithms use different sets of input data and optimization parameters. Occasionally we observed stagnation of the algorithm at a time-reversed version of the SH pulse. This case was readily identified by a higher mean square deviation between the reconstructed and measured cross-correlation function.

3.3 *Experimental setup and results*

The experimental setup for the SH pulse generation and characterization is shown in Fig. 4. The fundamental pulse source was a Kerr-lens mode-locked Ti:sapphire oscillator with a repetition rate of 88 MHz and an average power of 280 mW [2]. The output from the oscillator passed through a stretcher composed of two identical broadband antireflection-coated fused silica prisms (wedge angle of 10°) separated by 1 mm. Variable insertion of the prisms provided an adjustable path length and hence positive chirp on the FH pulses without beam displacement. The beam was loosely focused into the chirped-period-poled lithium tantalate (CPPLT) by a 1.42-mm-thick, 21 mm focal length BK7 lens to a spot size of 20 μm. Due to the compounded losses of the mirrors used for beam routing and the Fresnel reflection of the uncoated $LiTaO_3$ sample, only about 90 mW of the laser

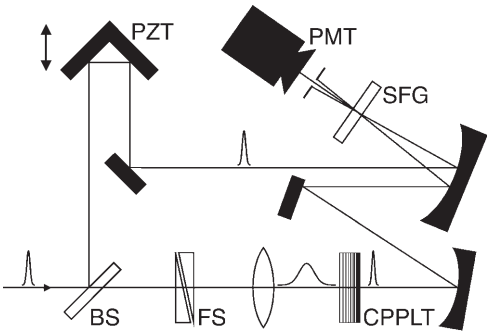

FIGURE 4 Experimental setup for generation and characterization of SH pulses. Note the exclusive use of reflective optics for the reference beam and the doubling-crystal output. BS, beam splitter; FS, adjustable fused-silica wedges; PZT, piezo-driven translation stage; SFG, crosscorrelation crystal; PMT, solar-blind photomultiplier

output arrived inside the CPPLT. The FH pulse acquired a total estimated chirp of $\sim 180\,\mathrm{fs}^2$ before entering the sample. The generated SH beam was collimated with a concave spherical aluminum-coated mirror of 50 mm radius of curvature. The SH output power was 0.41 mW inside and 0.35 mW after the CPPLT corresponding to an internal conversion efficiency of 0.45%/nJ. We attribute the difference in efficiency compared with the theoretical value of 2%/nJ to poling imperfections and the loose focusing employed.

For the characterization of the generated SH pulses, the CPPLT was placed in one arm of the cross-correlation setup. For the FH reference pulse, 8% of the FH power was split off before the stretcher with a 1-mm-thick fused silica beamsplitter oriented at 45° and passed through a delay line mounted on a piezoshaker. The SH beam and the FH reference beam were focused together by a concave 30 cm radius of curvature aluminum-coated mirror into a $< 10\,\mu$m-thick KDP crystal. The generated sum-frequency signal at around 270 nm passed through a Glan-Laser polarizer and an iris to reject the SH and the FH light and was then detected by a solar-blind photomultiplier. The position of the piezoshaker was calibrated with helium–neon laser interference fringes in a separate Michelson interferometer.

Before measurement of the cross-correlation, the chirp of the FH reference pulse was minimized at the location of the cross-correlation crystal, which was achieved by replacing the cross-correlation crystal with a 15-μm-thick ADP crystal and adjusting the dispersion between the laser and the cross-correlation setup to maximize the SH signal of the reference. Afterwards the dispersion of the prism stretcher before the CPPLT was adjusted for minimum cross-correlation width. The cross-correlation signal was recorded in a single sweep of the piezoshaker with an effective 11 bit digitization (Fig. 5). A high dynamic range is required in order to assure proper convergence of the decorrelation algorithms described above. The full width at half maximum (FWHM) of the trace shown in Fig. 5 is 12.7 fs.

The spectrum of the SH pulses was recorded with a spectrograph equipped with a 600 groove/mm grating and a UV-enhanced CCD camera (Fig. 6). The transform limit of this 220 THz bandwidth spectrum is 4.8 fs. The measured SH spectral shape deviates from the theoretically expected SH spectrum that is determined by the self-convolution of the FH

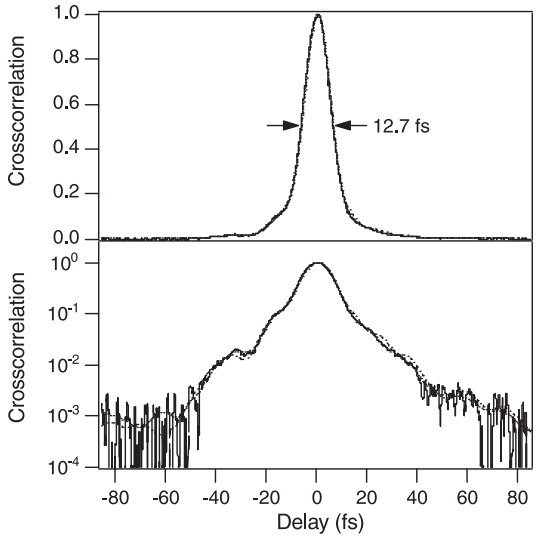

FIGURE 5 Measured cross-correlations (*solid curves*) on a linear (*top*) and a logarithmic scale (*bottom*). In addition to the measured data, the cross-correlations reconstructed by the two algorithms described in the text are shown (*dashed–dotted curve*, algorithm 1; *dotted curve*, algorithm 2)

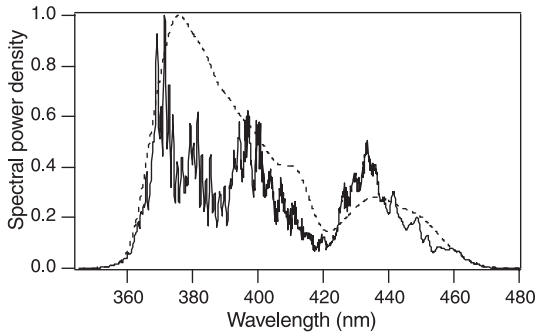

FIGURE 6 Measured SH power spectrum (*solid curve*) compared with the theoretically expected spectrum (*dashed curve*)

spectrum, which we tentatively attribute to poling imperfections in the QPM structure. It is important to note that such poling imperfections generally do not affect the phase of the generated SH pulse, but only its amplitude [14], the latter manifesting itself in the observed lower-than-ideal conversion efficiency. The origin of the rapidly varying spectral features is not fully understood but is not necessarily due the QPM nature of the device since a similar behavior has been observed using birefringent phase-matching [6]. We observed no indications of two-photon absorption or self-phase-modulation in the CPPLT.

The measured data was fed into the decorrelation algorithms described above. The SPIDER measurement of the reference pulse yielded a FWHM duration of 8.6 fs and a transform limit of 8 fs. This measurement is shown in Fig. 7 together with the fundamental spectrum. For comparison the fundamental pulse shape reconstructed by algorithm 2 is also included in this figure. The good agreement between the measured and reconstructed pulse shape is indicative of proper convergence of the algorithm. The reconstructed spectral phase of the SH pulse is depicted in Fig. 8. Excellent agreement was observed between the results from the two different algorithms. The rapid small-scale variation on the phase is a direct consequence of the experimental noise on

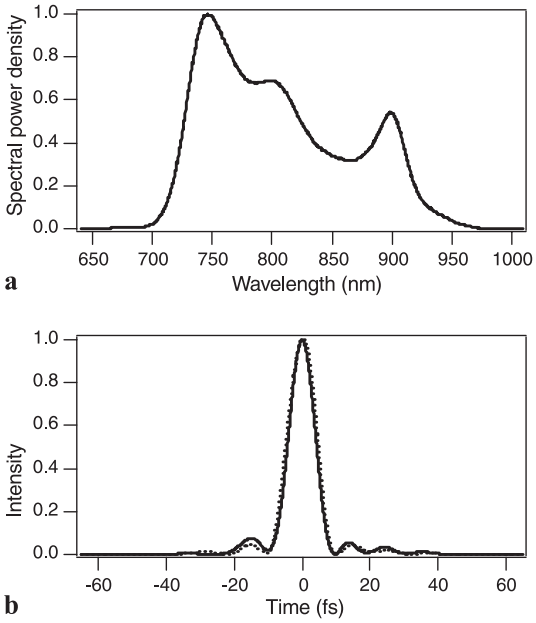

FIGURE 7 Fundamental power spectrum (*top*) and temporal pulse shape (*bottom*). The temporal pulse shape has been measured using spectral phase interferometry for direct electric field reconstruction (*solid curve*). For comparison the fundamental pulse reconstructed by decorrelation algorithm 2 is also shown (*dotted curve*)

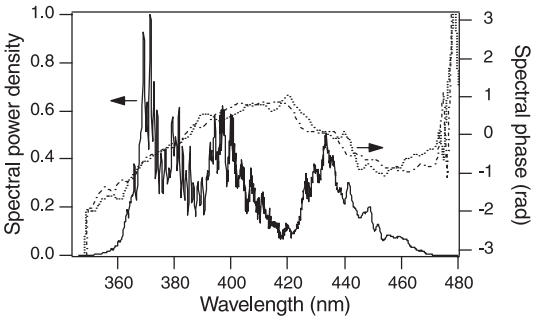

FIGURE 8 Spectral phase of the SH pulse as retrieved by the two decorrelation algorithms described in the text. The two phase functions agree excellently over the full wavelength range covered by the SH spectrum (*solid curve*). (*dashed–dotted curve*, algorithm 1; *dotted curve*, algorithm 2)

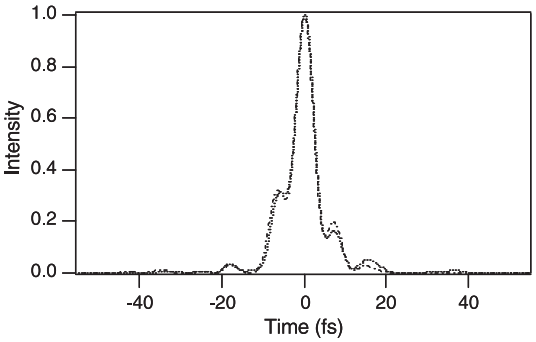

FIGURE 9 Temporal pulse shapes of the SH pulse reconstructed by the two decorrelation algorithms. The pulse duration corresponds to 5.2 fs for algorithm 1 (*dashed–dotted curve*) and 5.4 fs for algorithm 2 (*dotted curve*)

the input data. A Fourier transform of the reconstructed spectral phase together with the measured SH spectrum yields the corresponding temporal pulse shape (Fig. 9). The FWHM durations of the SH pulse shapes retrieved by the two algorithms were 5.2 fs and 5.4 fs, respectively. To our knowledge, these are the shortest pulses ever generated by SHG.

4 Conclusion

QPM-SHG pulse compression is an entirely scalable and engineerable approach to the frequency conversion of broadband pulses. No element providing negative dispersion other than the QPM crystal is needed to obtain short SH pulses. Thus, the experimental complexity is even lower than for conventional SHG using birefringent phase-matching. Stretching of the FH input pulse is achieved simply by passing the beam through an appropriate length of dispersive material. Using QPM-SHG pulse compression we were able to generate sub-6-fs pulses in the blue spectral region. The demonstrated approach allows scaling to even shorter blue pulses by using shorter FH pulses, because bandwidth and phase response are engineerable parameters. Larger conversion bandwidths can easily be obtained by scaling the QPM grating length. This is in strong contrast to birefringent phase-matching, where the crystal length generally limits the available bandwidth.

The conversion efficiency demonstrated so far is on the order of the values demonstrated for ultrashort-pulse birefringent SHG. But the FH pulses used in our experiment were relatively strongly chirped before entering the CPPLT. Efficiency of the SHG process scales with the FH peak power and can be improved by reducing the FH chirp in the grating design. Efficiencies of $\sim 20\%/\mathrm{nJ}$ are predicted for such designs. A particularly attractive design allows the generation of negatively chirped SH pulses. These pulses can then be compressed outside the nonlinear medium by passing through an appropriate length of positive dispersion material. An increased SH output chirp reduces the risk for two-photon absorption and should thus enable the scaling to higher output powers. QPM-SHG pulse compression opens up a new perspective for frequency conversion of ultrashort laser pulses. Beyond the demonstration of sub-10-fs pulses in this paper, this method can be adapted through a wide range of pulse energies, wavelengths, bandwidths and chirp configurations.

ACKNOWLEDGEMENTS The authors acknowledge financial support by the Swiss National Science Foundation and by the US Airforce Office of Scientific Research under Grant No. F49 620-99-1-0270.

REFERENCES

1 R. Ell, U. Morgner, F.X. Kärtner, J.G. Fujimoto, E.P. Ippen, V. Scheuer, G. Angelow, T. Tschudi, M.J. Lederer, A. Boiko, B. Luther-Davies: Opt. Lett. **26**, 373 (2001)
2 D.H. Sutter, G. Steinmeyer, L. Gallmann, N. Matuschek, F. Morier-Genoud, U. Keller, V. Scheuer, G. Angelow, T. Tschudi: Opt. Lett. **24**, 631 (1999)
3 G. Steinmeyer, D.H. Sutter, L. Gallmann, N. Matuschek, U. Keller: Science **286**, 1507 (1999)
4 O. Dühr, E.T.J. Nibbering, G. Korn, G. Tempea, F. Krausz: Opt. Lett. **24**, 34 (1999)
5 M. Wittmann, A. Nazarkin, G. Korn: Opt. Lett. **26**, 298 (2001)
6 A. Fürbach, T. Le, C. Spielmann, F. Krausz: Appl. Phys. B **70**, S37 (2000)
7 L. Gallmann, G. Steinmeyer, U. Keller, G. Imeshev, M.M. Fejer, J.-P. Meyn: Opt. Lett. **26**, 614 (2001)

8 A.M. Weiner: IEEE J. Quantum Electron. **QE-19**, 1276 (1983)
9 D. Steinbach, W. Hugel, M. Wegener: J. Opt. Soc. Am. B **15**, 1231 (1998)
10 J. Biegert, J.-C. Diels: J. Opt. Soc. Am. B **18**, 1218 (2001)
11 J.A. Armstrong, N. Bloembergen, J. Ducuing, P.S. Pershan: Phys. Rev. **127**, 1918 (1962)
12 M.M. Fejer, G.A. Magel, D.H. Jundt, R.L. Byer: IEEE J. Quantum Electron. **QE-28**, 2631 (1992)
13 M.A. Arbore, O. Marco, M.M. Fejer: Opt. Lett. **22**, 865 (1997)
14 G. Imeshev, M.A. Arbore, S. Kasriel, M.M. Fejer: J. Opt. Soc. Am. B **17**, 1420 (2000)
15 M.A. Arbore, A. Galvanauskas, D. Harter, M.H. Chou, M.M. Fejer: Opt. Lett. **22**, 1341 (1997)
16 G. Imeshev, A. Galvanauskas, D. Harter, M.A. Arbore, M. Proctor, M.M. Fejer: Opt. Lett. **23**, 864 (1998)
17 G. Imeshev, M.A. Arbore, M.M. Fejer, A. Galvanauskas, M. Fermann, D. Harter: J. Opt. Soc. Am. B **17**, 304 (2000)
18 A. Galvanauskas, D. Harter, M.A. Arbore, M.H. Chou, M.M. Fejer: Opt. Lett. **23**, 1695 (1998)
19 J.-P. Meyn, M.M. Fejer: Opt. Lett. **22**, 1214 (1997)
20 R. Trebino, K.W. DeLong, D.N. Fittinghoff, J. Sweetser, M.A. Krumbügel, B. Richman: Rev. Sci. Instrum. **68**, 1 (1997)
21 C. Iaconis, I.A. Walmsley: Opt. Lett. **23**, 792 (1998)
22 S. Linden, H. Giessen, J. Kuhl: Phys. Stat. Sol. B **206**, 119 (1998)
23 M. Zavelani-Rossi, G. Cerullo, S. De Silvestri, L. Gallmann, N. Matuschek, G. Steinmeyer, U. Keller, G. Angelow, V. Scheuer, T. Tschudi: Opt. Lett. **26**, 1155 (2001)
24 L. Gallmann, D.H. Sutter, N. Matuschek, G. Steinmeyer, U. Keller, C. Iaconis, I.A. Walmsley: Opt. Lett. **24**, 1314 (1999)
25 W.H. Press, S.A. Teukolsky, W.T. Vetterling, B.P. Flannery: *Numerical Recipes in C* (Cambridge University Press, Cambridge 1992)
26 A. Baltuska, A. Pugzlys, M.S. Pshenichnikov, D.A. Wiersma: 'Paper CWF22'. In: *Conf. on Lasers and Electro-Optics* (Optical Society of America 1999)